ACS APPLIED MATERIALS & INTERFACES
Research Article
www.acsami.org

Thermally Evaporated SiO Thin Films As a Versatile Interlayer for Plasma-Based OLED Passivation

Won Min Yun,[†] Jaeyoung Jang,[†] Sooji Nam,[†] Lae Ho Kim,[†] Sang Joon Seo,*,[‡] and Chan Eon Park*,[†]

[†]POSTECH Organic Electronics Laboratory, Polymer Research Institute, Department of Chemical Engineering, Pohang University of Science and Technology, Pohang, 790-784, Korea.

[‡]SKKU Advanced Institute of Nanotechnology (SAINT) and Center for Human Interface Nanotechnology (HINT), Sungkyunkwan University, Suwon 440-746, Republic of Korea.

Supporting Information

ABSTRACT: Silicon monoxide (SiO) thin films were introduced as an efficient interlayer for achieving plasma-based organic light-emitting diode (OLED) surface passivation. The SiO thin films could be consecutively formed via thermal evaporation, without breaking the vacuum, after deposition of the OLED cathode. The plasma resistivity and UV-blocking characteristics of the SiO interlayer protected the OLED devices against electrical and optical degradation during the plasma-enhanced atomic layer deposition (PEALD) and plasma-enhanced chemical vapor deposition (PECVD) passivation processes. In addition, the nonconformal deposition and hydroxyl group-rich surface characteristics of the SiO thin films yielded enhanced surface pinhole coverage and a higher initial film density in the subsequently deposited PEALD-based Al_2O_3 barrier film. As a result, the OLEDs with a SiO/Al_2O_3 bilayer passivation layer displayed a remarkably increased device shelf life compared to devices prepared using Al_2O_3-only passivation. A MOCON test showed that the water vapor transmission rate (WVTR) of the SiO/Al_2O_3 bilayer film was 0.0033 g/(m^2 day), 2.3 times lower than the rate of a single Al_2O_3 barrier film. The results of our study demonstrated the multipurpose role of a SiO interlayer in plasma-based OLED passivation. The layer acted as a damage-free protective layer for the underlying OLED devices and an assistant layer to improve the upper barrier film performance.

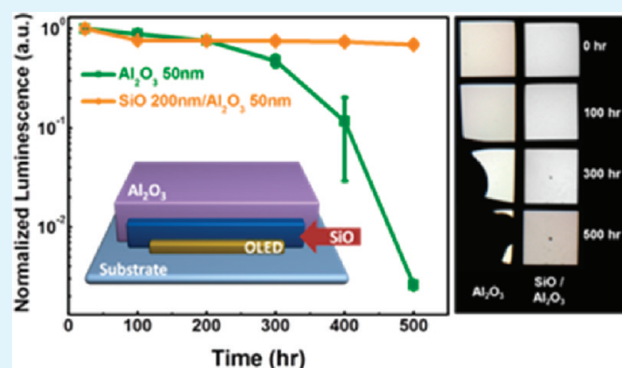

KEYWORDS: *organic light emitting diodes (OLEDs), thin film encapsulation, protective interlayer, barrier property enhancement, silicon monoxide (SiO), passivation*

1. INTRODUCTION

Ever because of the first reported preparation of heterostructured bilayer organic light-emitting diodes (OLEDs),[1] extensive research has been performed in an effort to improve the performance and stability of OLEDs. OLEDs display several excellent properties that are appropriate for use in flat panel displays (FDPs), such as the small thickness, low power consumption, wide viewing angle, and mechanical flexibility.[2,3] As a result of steady research progress, OLEDs are now entering into commercialization, and their market utility is growing.[4] The intrinsic vulnerability of organic active layers and the cathodes of OLEDs toward oxygen and water vapor in air suggests the need for hermetic encapsulation of OLED devices. Glass caps are widely used in commercialized OLEDs products;[5] however, although glass caps satisfy the water permeation requirements of OLEDs (1×10^{-6} g/(m^2 day)),[6] glass caps hinder the realization of potential OLED applications, including the preparation of extremely slim mechanically flexible lightweight displays because of the large form factor and rigidity of glass.[7] To overcome these drawbacks, thin film passivation approaches that employ direct deposition techniques to produce thin film barriers into OLEDs have been suggested as an alternative method for achieving OLED passivation.[7] Thin film passivation systems have been tested by depositing single layers of inorganic materials, such as SiO_2,[8] Si_3N_4,[8] Al_2O_3,[9−12] nanolaminated inorganic layers[13−15] and inorganic/organic multilayers[6,16,17] have been tested as OLED barrier films. Inorganic barrier thin film deposition is preferably achieved using plasma-based deposition methods (PECVD, PEALD) rather than thermal deposition methods (thermal CVD, thermal ALD) because these approaches yield the highest quality films and minimize the thermal damage to the organic materials during the deposition process; however, the gas plasma, a reactive ion used in plasma-based deposition, can also deteriorate the organic active layers.[18] Therefore, an appropriate protective layer between the OLEDs and the

Received: April 6, 2012
Accepted: May 31, 2012
Published: May 31, 2012

© 2012 American Chemical Society

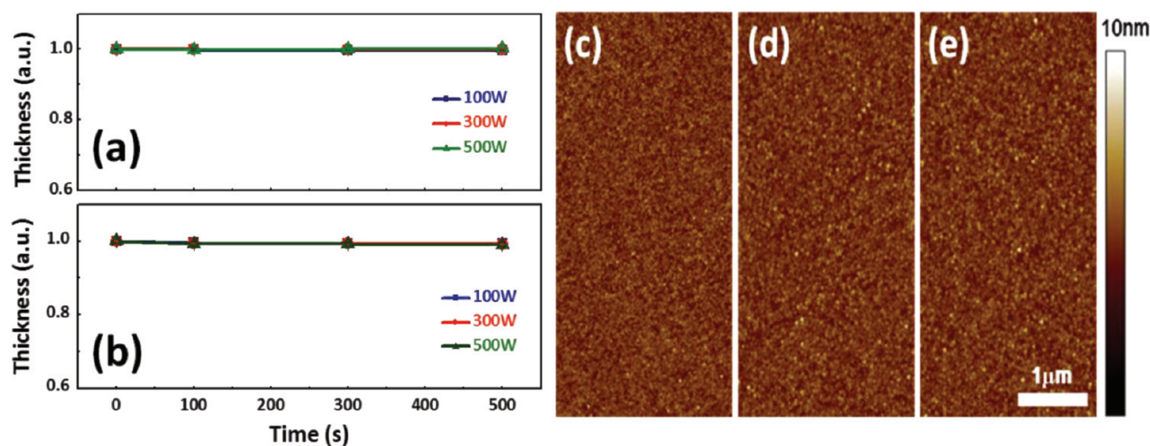

Figure 1. Thickness variations of the 200 nm SiO layers prepared under (a) argon or (b) oxygen plasma treatment. Surface morphologies of the pristine (c) SiO, (d) argon-etched, and (e) oxygen-etched layers.

passivation layers is required to maintain both the electrical and optical properties of OLEDs during passivation. For this purpose, in 2008, Wong et al. reported the use of a copper phthalocyanine (CuPc) interlayer between the OLEDs and the plasma-enhanced chemical vapor deposition (PECVD)-based SiN_x barrier film. The plasma damage to the OLEDs was reduced and the barrier properties of the upper barrier film were enhanced;[19] however, the interlayer used, CuPc, was an organic material that does not guarantee sufficient plasma resistivity.

In addition to plasma damage protection, UV-blocking characteristics are also required of a passivation interlayer to prevent UV light from penetrating the OLEDs because UV light can be a source of photo-oxidation of organic active layers.[20] Any implementation of UV-blocking characteristics must simultaneously maintain the transmittance in the visible region. UV curable polymers are generally used as organic materials in inorganic/organic multistack passivation processes (the most efficient passivation configuration up to now). Hence, OLEDs may be exposed to intense UV light during the monomer curing step; therefore, the use of appropriate UV-blocking layers is important in this field.

Here, we introduce the use of thermally evaporated silicon monoxide (SiO) thin films as a protective interlayer for achieving plasma-based OLED passivation, including PEALD and PECVD. After OLED cathode deposition, the SiO thin films can be sequentially formed without breaking the vacuum. The resulting SiO films displayed good resistivity toward argon (Ar) and oxygen (O_2) plasmas and exhibited good UV-blocking characteristics at 254 nm with transparency over the visible region. Furthermore, the SiO films showed good compatibility with the upper barrier film, the PEALD-based Al_2O_3, because of the increased pinhole coverage and the hydroxyl group-rich surface characteristics. The device shelf-lives of the OLEDs prepared using SiO/Al_2O_3 bilayer passivation were significantly enhanced compared to the shelf-lives of devices prepared using Al_2O_3-only passivation, as a result of the improved water vapor transmittance rate of the Al_2O_3/SiO bilayer films.

2. EXPERIMENTAL SECTION

Materials and Sample Preparation. Silicon monoxide (SiO) was purchased from TASCO Inc. (99.97%) and was used as received without further purification. It was deposited using a metal evaporator incorporated into a cluster-type OLED fabrication system (SUNIC SUNICEL 0603). The SiO deposition rate was fixed at 1 Å/s in all experiments under 5×10^{-6} Torr vacuum. Basic information (density and % composition) for vacuum thermally deposited SiO was available in the Supporting Information, Figures S1 and S2. Ar, O_2, and CF_4 plasma etching was performed using an inductively coupled plasma (ICP) etcher (SNTEK ICP1000). The process pressure and gas flow were fixed at 20 mTorr and 20 sccm, respectively. The OLEDs were fabricated using an octagonal cluster-type evaporating system (SUNIC SUNICEL 0603) under a vacuum of less than 5×10^{-6} Torr. The vacuum was not broken during fabrication. Indium tin oxide (ITO) with a sheet resistance of 14 Ω/sq was coated onto glass to provide a substrate for the bottom-emission OLEDs. ITO was prepatterned to form the electrodes, and the photoresist was coated to define the pixels using conventional photolithography. After UV-ozone treatment of a precleaned ITO substrate, the organic layers and metallic cathode were deposited in the configuration of ITO 150 nm/MoO_x 3 nm, to provide a hole injection layer/NPB (a-naphthylphenylbiphenyl) 50 nm hole transport layer/Alq_3 (tris(8-quinolato) aluminum) (C545T (10-(2-benzothiazolyl)-2,3,6,7-tetrahydro-1,1,7,7-tetramethyl -1H, 5H,11H-(1)-benzopyropyrano (6,7-8-i,j) quinolizin-11-one) 2% doped) 30 nm emission layer/Alq_3 20 nm electron transport layer/Liq (quinolato lithium) 1 nm electron injection layer/Al 120 nm. The permeation barrier film was prepared by depositing, respectively, SiN_x and Al_2O_3 thin films via PECVD (BMR technology Hidep-SC) and PEALD (Quros 200). For SiN_x deposition, SiH_4, NH_3, and Ar gases were used, respectively, as the Si source, N source, and diluent gas. A total of 300 W radio frequency (RF) power was applied to enable plasma generation, and the internal pressure was set to 20 mTorr during the deposition process. For Al_2O_3 deposition, trimethyl aluminum (TMA) and O_2 were used as reactive sources for Al and O, respectively. RF power of 100 W with a 20 μs pulse width was used, and the chamber temperature was set to 100 °C to ensure the organic thermal stability of the OLEDs during Al_2O_3 deposition.

Characterization. The thickness variations after plasma etching were measured using a spectroscopic ellipsometer (J. A. Woollam M200D). Current density−voltage−luminescence ($J-V-L$) measurements of the OLEDs were performed using a homemade system incorporating a Keithley 236 current source and a Minolta CS1000 luminescence meter. Shelf-life time and emission area images were measured at 10.8 mA/cm^2 constant current density condition with 1000 ± 50 cd/m^2 of initial luminescence. The surface morphology was measured using an atomic force microscope (VEECO dimension 3100) and a scanning electron microscope (JEOL JSM 7401F). The photoluminescence (PL) decay of the UV-exposed Alq_3 thin films were measured using a PL measurement system (Jasco FR650). The WVTR was obtained using an MOCON AQUATRAN-1. X-ray photoemission spectroscopy (XPS) was performed using an Escalab 220IXL.

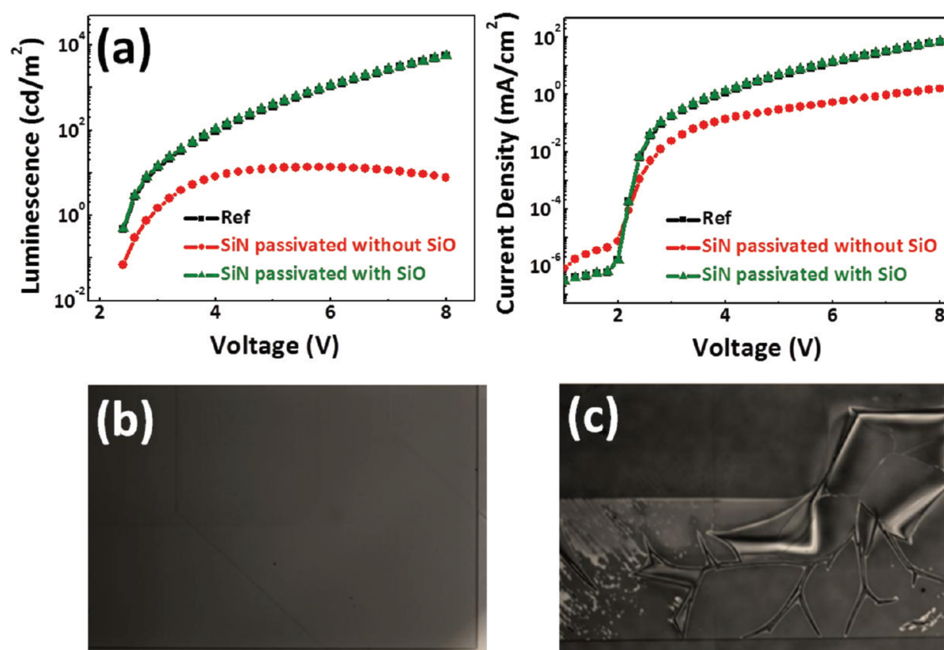

Figure 2. (a) $J-V-L$ characteristics of the OLED devices before and after PECVD-based SiN_x 200 nm deposition with and without 200 nm SiO interlayer. Optical microscopy images of SiNx-deposited OLED devices (b) with a SiO interlayer or (c) without a SiO interlayer.

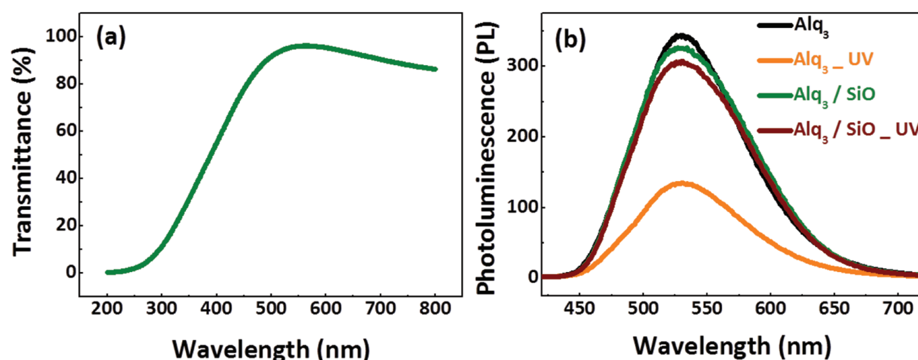

Figure 3. (a) UV−vis transmittance of SiO 200 nm deposited on a quartz substrate. (b) UV-induced photo-oxidation characteristics of Alq_3 with or without a SiO interlayer.

3. RESULTS AND DISCUSSION

The plasma resistivity of the SiO interlayer was investigated by depositing 200 nm thick SiO thin films onto wafers via thermal evaporation, followed by exposure to O_2 and Ar plasma for 500 s under a variety of power conditions (100, 300, and 500 W). As shown in Figures 1a and 1b, the thickness variations of the SiO thin films were less than 0.1%, even after the extremely harsh conditions (up to 500 W for 500 s) associated with the ICP treatment using both O_2 and Ar gases. The surface morphologies of the bare and plasma-treated SiO films were examined by AFM (see Figures 1c−e). As illustrated in the AFM topographs, no significant changes in the surface morphologies were observed after ICP treatment, and the root-mean-square roughness values (R_q) were nearly identical: the R_q values of the bare SiO films, Ar plasma-treated films, and O_2 plasma-treated films were 0.6 nm, 0.583 nm, and 0.539 nm, respectively.

To further examine the effects of the plasma during passivation on the OLED performance, we fabricated OLED devices (structure: ITO 150mn/MoO_x 3 nm/NPB 60 nm/Alq3 (C545T 2%) 30 nm/Alq3 20 nm/Liq 1 nm/Al 15 nm) and deposited 200 nm thick SiN_x layers via PECVD directly onto the devices with and without a SiO interlayer. As shown in the optical microscopy image presented in Figure 2b, the SiN_x film displayed a smooth morphology and good surface coverage in the SiO interlayer-deposited OLEDs. Moreover, the $J-V-L$ characteristics were nearly identical before and after the SiNx layer deposition (see Figure 2a). On the other hand, dramatic surface deformations at the organic/SiNx interface (i.e., cracks or delamination) were observed for the SiNx film on the OLEDs without a SiO interlayer, as shown in the optical microscopy image of Figure 2c. As shown in Figure 2a, we also confirmed drastic deformation of $J-V-L$ characteristic of OLEDs without SiO interlayer (Max luminescence was ∼15 cd/m^2). We speculated that this device performance degradation originated from plasma damage to the underlying OLED devices during the PECVD process. These results confirmed the excellent plasma resistivity of the SiO interlayer.

The optical properties of the SiO interlayer film were evaluated by depositing 200 nm thick SiO thin films onto a quartz substrate, after which the UV−vis transmittance was measured. As shown in Figure 3a, the SiO thin films showed

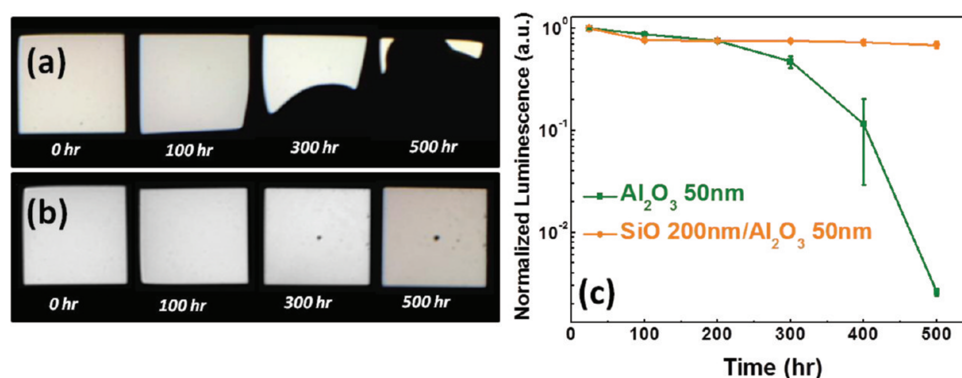

Figure 4. Emitting area images of a (a) 50 nm Al_2O_3-passivated OLED, and (b) a SiO 200 nm/Al_2O_3 50 nm-passivated OLED. (c) Shelf-lives of the Al_2O_3-only and SiO/Al_2O_3-passivated devices. (60 °C, 90% RH condition).

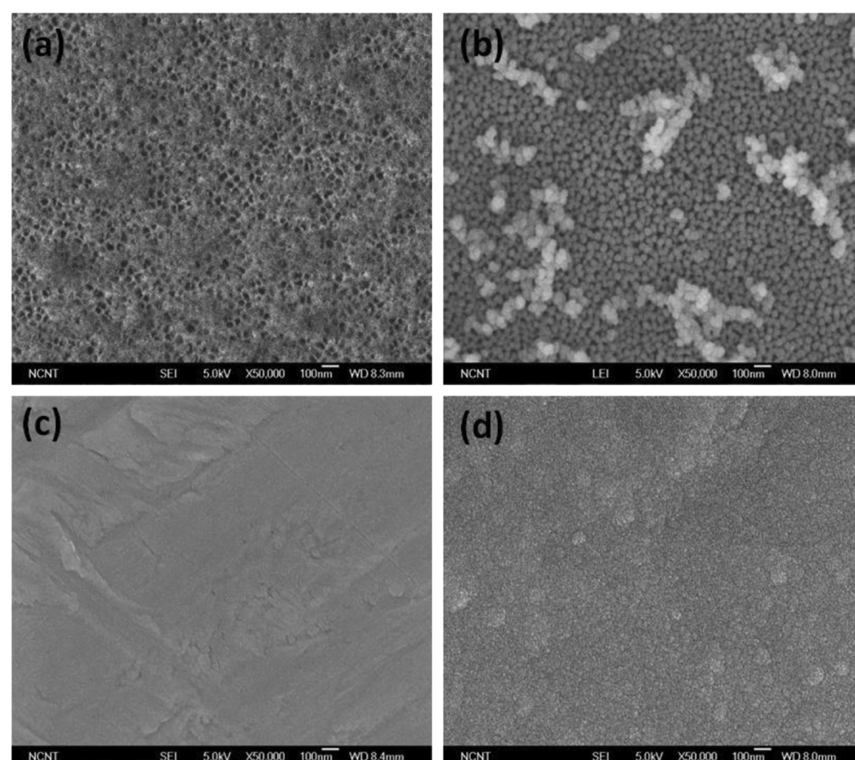

Figure 5. FE-SEM images of (a) a pristine AAO substrate (20 nm pores) and (b) 50 nm SiO-deposited AAO, (c) 100 nm SiO-deposited AAO, (d) 200 nm SiO-deposited AAO.

less than 5% transmittance in the deep UV region (at 254 nm); however, over the visible region (400–800 nm), although a small absorption band was observed in the near-UV (around 400 nm), an average transmittance of 88.9% was obtained. The transparency in the visible region and the UV-blocking characteristics of the SiO thin films suggested their suitability as passivation interlayers. Since the visible light penetrated into the interlayer without incurring significant losses, the SiO interlayer may be applicable to top-emission OLED device passivation. Simultaneously, the interlayer may protect the OLEDs from possible UV-induced photo-oxidation of the organic active layers in OLEDs due to the UV-blocking characteristics.[20] The UV-blocking characteristics of the SiO thin films were confirmed again by measuring the PL decay of the Alq_3 thin films with and without SiO thin films (sample configuration: quartz substrate/SiO 200 nm/Alq_3 300 nm and quartz substrate/Alq_3 300 nm). UV light, 254 nm in wavelength, was introduced onto the samples from the quartz side over 300 min, and the corresponding PL intensities were measured from the Alq_3 side in an effort to exclude the SiO effects on the PL intensity. As shown in Figure 3b, the PL intensity of the Alq_3 thin films without a SiO interlayer was dramatically reduced after 300 min of UV irradiation (to 40% of the PL intensity of the unexposed film). On the other hand, the Alq_3 thin films with a SiO interlayer exhibited only slight degradation of the PL intensity, approaching the results of the natural PL degradation of Alq_3 in ambient air over 5 h. These results indicate that the SiO interlayer can act as an effective optical barrier and protect the organic active materials from UV radiation damage.

Device application tests of the SiO interlayer were conducted by measuring the shelf-lives of the OLEDs under ambient dark conditions (RH: 90%). After device fabrication, thin film passivation was performed by depositing 50 nm thick Al_2O_3

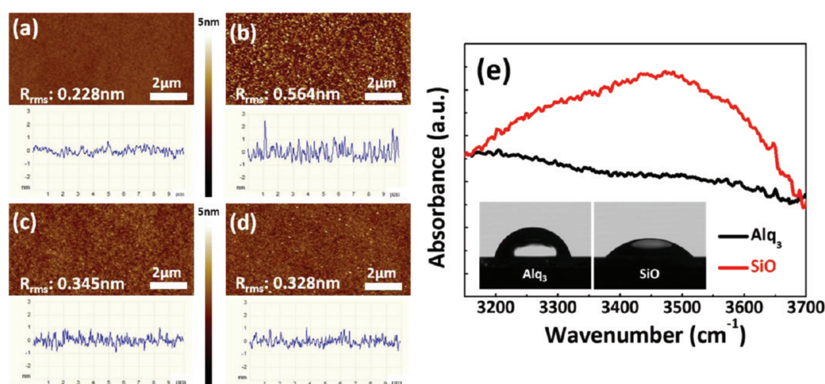

Figure 6. AFM images of the pristine surfaces of (a) the Alq_3 100 nm/Al_2O_3 1 nm and (b) CF_4 plasma-etched surfaces of Alq_3 100 nm/Al_2O_3 1 nm. AFM images of (c) the pristine surfaces of SiO 100 nm/Al_2O_3 1 nm and (d) CF_4 plasma-etched surfaces of SiO 100 nm/Al_2O_3 1 nm. (e) FT-IR absorbance for SiO 300 nm and Alq_3 300 nm (−OH region) and water contact angle for Alq_3 and SiO (inset).

thin films via PEALD onto the OLED devices either with or without a SiO interlayer. Images a and b in Figure 4 show digital camera images of the emitting area of the OLED devices over time. As plotted in Figure 4c, the device with a SiO interlayer showed an extended shelf life relative to devices prepared using the Al_2O_3-only passivation layer. Moreover, the devices without a SiO interlayer showed distinct predominant edge shrinkage degradation, and eventually all emissive regions became nonemissive after 500 h storage. Dark spot formation was observed in the center of SiO/Al_2O_3 passivated devices after 300 h storage, we speculated that gigantic dust particle over several micrometer diameters, which cannot be covered by SiO 200 nm, was incorporated during the passivation process. However, even with this large dust particle, SiO/Al_2O_3 barrier film sustained their property up to 300 h and growth rate of dark spot radius is quite lower than the emission area degradation speed of without SiO layer. The WVTR data revealed that the WVTR of the SiO/Al_2O_3 bilayer film (0.0033 g/m^2day) was 2.3 times lower than that of the single Al_2O_3 film (0.0076 g/m^2day) (sample configuration: polyethylene naphthalate (PEN) 200 μm/SiO 200 nm/Al_2O_3 50 nm and PEN 200 μm/Al_2O_3 50 nm). The enhanced barrier properties were attributed to the additional barrier property of the SiO interlayer; however, the WVTR obtained for the 200 nm thick SiO thin films was only 0.621 g/m^2day. According to the ideal laminate theory, the permeation rate of a multilayer can be predicted from the permeation rates of each film.[21] In the SiO/Al_2O_3 system, the total permeation rate could be derived from the equation shown below:

$$\frac{1}{P_{\text{total}}} = \frac{1}{P_{\text{SiO}}} + \frac{1}{P_{\text{Al}_2\text{O}_3}}$$

This equation predicts that the permeation rate of the SiO/Al_2O_3 film is 0.0075 g/m^2day should be greater than 2 times the measured WVTR of the SiO/Al_2O_3 film. These results indicate that the individual film characteristics of the SiO/Al_2O_3 bilayer differ from those of each homogeneous single film; therefore, we speculate that the barrier properties may be enhanced by introducing certain features at the interfaces between (1) the OLEDs and the SiO layer, and (2) the SiO and Al_2O_3 layers. On the basis of these considerations, we hypothesize that these improvements resulted from (1) the increased surface pinhole coverage due to the presence of the thermally evaporated SiO interlayer; and (2) the enhanced initial film density and coverage of the plasma-based barrier film on the SiO interlayer.

The ability of the SiO thin films to cover pinholes was investigated using a 20 nm pore-sized anodized aluminum oxide (AAO) substrate with 50 μm thickness (Whatman co.) as the pseudopinhole-rich surface. Figure 5a shows a SEM image of an AAO surface in which 20 nm pore-sized pinholes may be clearly seen over the entire surface area. After thermal evaporation of the 100 nm thick SiO thin films onto the AAO surfaces, nearly all pinholes were covered with the SiO layers, and the surface appeared to be remarkably smooth (Figure 5c). Surface coverage of the SiO on AAO substrate with various thicknesses was also investigated using FE-SEM measurement. According to Figure 5b,d, with 50 nm deposition of SiO showed pinholes with shrunk pore size. In addition, 200 nm SiO deposited AAO showed no AAO pinholes on the surface as 100 nm deposited AAO. From these images, we can conclude that nonconformal deposition of SiO grew around pinhole fringe and finally cover the pinholes even though pinhole depth is quite deep. Pinholes can provide a main pathway for water vapor permeation and can introduce barrier film discontinuities and crack formation.[22] By covering the abnormalities, such as the pinholes, cracks, and dust particles on the surface of the OLEDs, the device surfaces with an SiO interlayer display improved permeation barrier characteristics for the SiO/Al_2O_3 bilayer films. Because thermal evaporation is a nonconformal deposition method, the deposited film did not grow along the surface structure, unlike films deposited using conformal deposition methods, such as ALD or CVD. Hence, a thermally evaporated SiO interlayer with a proper thickness could cover the surface cracks or pinholes. By introducing a SiO interlayer prior to the conformal deposition of Al_2O_3 via PEALD, the intrinsic pinholes and defects may be reduced, and the barrier properties may be improved.

In addition to the pinhole-coverage effects, the SiO interlayer can increase the initial surface coverage and density of the PEALD-based Al_2O_3 barrier film because of the −OH group-rich surface characteristics of SiO films. To investigate the initial properties of the Al_2O_3, 1 nm thick Al_2O_3 thin film deposited onto the SiO film was compared with one deposited onto an organic material (Alq_3). Subsequently, CF_4 plasma (which etches SiO and organic materials but does not etch aluminum compounds, such as Al_2O_3) was used to perform the etching step. We therefore examined the initial coverage and density of the PEALD-based Al_2O_3 thin films on the SiO and Alq_3 thin films, by investigating the variations in the surface morphology of the Al_2O_3 films on both surfaces before and

dx.doi.org/10.1021/am300600s | ACS Appl. Mater. Interfaces 2012, 4, 3247−3253

after CF_4 plasma etching. Figure 6a and 6c show the AFM topographs of the as-deposited 1 nm thick Al_2O_3 films on the Alq_3 and SiO layers, respectively. After 1000 s CF_4 plasma etching, the Al_2O_3 films on the SiO layers showed negligible changes in the surface roughness (from 0.345 to 0.328 nm); however, the Al_2O_3 films on the Alq_3 layers yielded more than a 2-fold increase in the surface roughness (from 0.228 to 0.564 nm) (see Figures 6b and 6d, respectively). These variations are more clearly depicted in the cross-sectional height profiles of each AFM topograph, as shown in Figure 6. The presence of the Al_2O_3 films was investigated by measuring the surface atomic contents of both samples after CF_4 plasma etching using XPS. An Al atomic content exceeding 30% was confirmed in both cases, indicating the presence of the Al_2O_3 film, even after CF_4 plasma etching (data not shown). Therefore, the increase in the surface roughness was mainly due to the plasma-exposed organic regions over which the Al_2O_3 films were not fully covered. This difference in the initial surface coverage of the Al_2O_3 film originates from differences in the density of surface −OH groups in the underlying films, the SiO and Alq_3 layers. During Al_2O_3 deposition using TMA as an Al source, the substrate surface −OH groups act as preferred initiation sites for film growth.[23] For confirming relative amount of surface −OH, we measured reflection mode FT-IR for hydroxyl group detection about SiO 300 nm and Alq_3 300 nm on Al coated Si wafer, respectively. As shown Figure 6e, in −OH peak region (3200−3700 cm^{-1}), SiO show higher absorbance than Alq_3. In addition, inset of Figure 6e shows the water contact angle of the SiO and Alq_3 surfaces, respectively. The water contact angles of SiO and Alq_3 were found to be 40° and 68°, respectively. These FT-IR and contact angle results suggest that the SiO thin films provide −OH group-rich surfaces for the PEALD process, which leads to the improved initial surface coverage and density of the upper Al_2O_3 film. Our conclusion was confirmed by measuring the WVTR values of the Al_2O_3 films initially deposited onto the SiO or Alq_3 layers. Table 1 summarizes the MOCON test results of 1, 3, 5, 10, and 50 nm thick Al_2O_3 films deposited onto PEN 200 μm/Alq_3 200 nm or PEN 200 μm/SiO 200 nm, respectively. Using only 3 nm Al_2O_3 deposition layers on the SiO surface, the bilayer film reached a critical thickness, at which point the WVTR value was maintained at a constant level. By contrast, the Al_2O_3 film deposited onto the organic Alq_3 surface did not meet the critical thickness condition by a thickness deviation of 10 nm.[5] These MOCON results indicated that the Al_2O_3 films deposited onto the SiO surface, thereby effectively cover the underlying SiO layer during initial stages of deposition (3 nm). Their bulk characteristics appeared to be thinner thickness than those of the Al_2O_3 film deposited onto Alq_3. The results shown above suggest that the −OH group-rich surface characteristics of the SiO interlayer improved the initial barrier characteristics and surface coverage of the upper Al_2O_3 films; thereby increasing the barrier properties of the SiO/Al_2O_3 bilayer films.

Table 1. Water Vapor Transmission Rate (WVTR) of Al_2O_3 Layers with 0−50 nm Thicknesses on PEN/Alq_3 and PEN/SiO Substrates (WVTR of PEN Substrate: 1.307 g/(m^2 day))

	WVTR (g/(m^2day))					
	bare	Al_2O_3 1 nm	Al_2O_3 3 nm	Al_2O_3 5 nm	Al_2O_3 10 nm	Al_2O_3 50 nm
Alq_3 200 nm	0.713	0.678	0.0207	0.0183	0.00528	0.00551
SiO 200 nm	0.621	0.4	0.0074	0.00652	0.0046	0.0033

4. CONCLUSIONS

In conclusion, we introduced thermally evaporated SiO thin films as a versatile and efficient interlayer for plasma-based OLED passivation. The plasma resistivity and UV-blocking characteristics of the SiO interlayer enabled formation of excellent upper barrier films in the OLED devices, as well as plasma-based PECVD or PEALD deposition methods without deteriorating optical and electrical properties. Experimental studies revealed that the nonconformal deposition and hydroxyl group-rich surface characteristics of the SiO thin films enhanced the surface pinhole coverage and the initial film density of the upper Al_2O_3 barrier film. In addition, the WVTR data associated with the SiO/Al_2O_3 bilayer films displayed remarkable improvements compared with the single Al_2O_3 films. The device shelf-lives of the OLEDs prepared with SiO/Al_2O_3 bilayer passivation were significantly enhanced. Our work confirmed that the use of SiO interlayers in plasma-based OLED passivation provides a facile route to preparing high-quality thin film passivation for use in OLED devices.

■ ASSOCIATED CONTENT

Ⓢ Supporting Information

Basic information about vacuum thermally evaporated SiO film (at % composition of Si and O with XPS measurement, deposited SiO film density with XRR measurement and simulated data). This material is available free of charge via the Internet at http://pubs.acs.org/.

■ AUTHOR INFORMATION

Corresponding Author

*E-mail: cep@postech.ac.kr (C.E.P); sjoonseo@skku.edu (S.J.S.).

Notes

The authors declare no competing financial interest.

■ ACKNOWLEDGMENTS

This work was supported by the RFID R&D program of MKE/KEIT. [10035225, Development of core technology for high-performance AMOLEDS on plastic.]

■ REFERENCES

(1) Tang, C. W.; Van Slyke, S. A. *Appl. Phys. Lett.* **1987**, *51*, 913−915.

(2) Gross, M.; Muller, D. C.; Nothofer, H. G.; Scherf, U.; Neher, D.; Brauchle, C.; Meerholz, K. *Nature* **2000**, *405*, 661−665.

(3) Brown, A. R.; Marks, R. N.; Mackay, K.; Friend, R. H.; Burns, P. L.; Holmes, A. B. *Nature)* **1990**, *347*, 539−541.

(4) Liao, K. OLED market outlook. *Technical Report DisplaySearch*; DisplaySearch: Santa Clara, CA, 2008

(5) Burrows, P. E.; Bulovic, V.; Forrest, S. R.; Sapochak, L. S.; McCarty, D. M.; Thompson, M. E. *Appl. Phys. Lett.* **1994**, *65*, 2922−2924.

(6) Burrows, P. E.; Graff, G. L.; Gross, M. E.; Martin, P. M.; Shi, M. K.; Hall, M.; Mast, E.; Bonham, C.; Bennet, W.; Sullivan, M. B. *Displays* **2001**, *22*, 65−69.

(7) Lewis, S. J.; Weaver, S. M. *IEEE J. Sel. Top. Quantum Electron.* **2004**, *10*, 45−57.

(8) Sobrinho, A. S.; Czeremuszkin, G.; Latrache, M.; Wertheimer, M. R. *J. Vac. Sci. Technol., A.* **2000**, *18*, 149−157.

(9) Carcia, P F.; McLean, R. S.; Reilly, M. H.; Groner, M. D.; George, S. M. *Appl. Phys. Lett.* **2006**, *89*, 031915.

(10) Park, S. H.; Oh, J.; Hwang, C. S.; Lee, J. I.; Yang, Y. S.; Chu, H. Y. *Electrochem. Solid-State Lett.* **2005**, *8*, H21−H23.
(11) Langereis, E.; Creatore, M.; Heil, S. B. S.; Van de Sanden, M. C. M.; Kessels, W. M .M. *Appl. Phys. Lett.* **2006**, *89*, 081915.
(12) Carcia, P. F.; McLean, R. S.; Reilly, M. H.; Groner, M. D.; George, S. M. *Appl. Phys. Lett.* **2006**, *89*, 031915.
(13) Meyer, J.; Schneidenbach, D.; Winkler, T.; Hamwi, S.; Weimann, T.; Hinze, P.; Ammermann, S.; Johannes, H.; Riedl, T.; Kowalsky, W. *Appl. Phys. Lett.* **2009**, *94*, 233305.
(14) Meyer, J.; Gorrn, P.; Bertram, F.; Hamwi, S.; Winkler, T.; Johannes, H.; Weimann, T.; Hinze, P.; Riedl, T.; Kowalsky, W. *Adv. Mater.* **2009**, *21*, 1845−1849.
(15) Dameron, A.; Davidson, S.; Burton, B.; Carcia, P.; McLean, R.; George, S. M. *J. Phys. Chem. C* **2008**, *112*, 4573−4580.
(16) Dameron, A. A.; Saghete, D.; Burton, B. B.; Davison., S. D.; Cananagh, A. S.; Bertand, J. A.; George, S. M. *Chem. Mater.* **2008**, *20*, 3315−3326.
(17) Han, Y. C.; Jang, C.; Kim, K. J.; Choi, K. C.; Jung, K. H.; Bae, B. S. *Org. Electron.* **2011**, *12*, 609−613.
(18) Mattox, D. M. *J. Vac. Sci. Technol.* **1989**, *A 7*, 1105−1114.
(19) Wong, F. L.; Fung, M. K.; Tao, S. L.; Lai, S. L.; Tsang, W. M.; Kong, K. H.; Choy, W. M.; Lee, C. S.; Lee, S. T. *J. Appl. Phys.* **2008**, *104*, 014509.
(20) Wang, X. Z.; Gao, X. D.; Zhou, Y. C.; Xie, Z. T.; Song, Q. L.; Ding, X. M.; Hou, X. Y. *Thin Solid Films* **2008**, *516*, 2171−2174.
(21) Graff, G. L.; Williford, R. E.; Burrows, P. E. *J. Appl. Phys.* **2004**, *96*, 1840−1849.
(22) Greener, J.; Ng, K. C.; Vaeth, K. M.; Smith, T. M. *J. Appl. Polym. Sci.* **2007**, *106*, 3534−3542.
(23) Ghosh, M. K.; Choi, C. H. *Chem. Phys. Lett.* **2006**, *426*, 365−369.